Testing the applicability of standardised growth curves (SGC) for chemically heterogeneous single-grain feldspars from the Atacama Desert, Chile

Linda A.E. Maßon[1*], Svenja Riedesel[1,2], Anja Zander[1], Mariana Sontag-González[3,4], Tony Reimann[1]

[1] Institute of Geography, University of Cologne, Germany

[2] Radiation Physics Division, Department of Physics, Technical University of Denmark, Denmark

[3] Institute of Geography, Justus-Liebig-University Gießen, Germany

[4] Department of Geosciences, Stony Brook University, NY 11794-2100, USA

* Correspondence: l.masson@uni-koeln.de

Keywords:

Feldspar, single grain pIRIR, standardised growth curve, Atacama Desert, single grain geochemistry

Abstract

The Atacama Desert is generally considered the driest non-polar desert on Earth and is therefore an ideal study area for exploring the water and biota free endmember of Earth's Critical Zone (ECZ). Single grain (SG) luminescence dating has successfully identified processes in the ECZ. However, SG luminescence dating of Atacama Desert feldspars is challenging and time consuming since only a small fraction of grains emits sufficient luminescence and their potassium (K) contents, needed for internal dose rate calculations, are highly variable. Here we present an adaption of the standardised growth curve (SGC) method adjusted to the conditions of Atacama Desert sediments and a correlation of single-grain geochemistry and luminescence properties.

To evaluate if SGCs are suitable for our study site and to determine the influence of the K-content on our luminescence age calculations, we used a set of five samples from the Atacama Desert and five chemically and structurally different feldspar sediment extracts from various geological origins worldwide. We performed a dose recovery test (DRT) using a post-infrared infrared stimulated luminescence (pIRIR) protocol and measured nine major element concentrations, including K, on a single grain level using a scanning electron microscope (SEM) with energy-dispersive X-ray spectroscopy (EDX). The DRT dataset was then used to test the application of SGCs. The accuracy of Atacama feldspar pIRIR measurements fitted onto SGCs frequently suffers from outliers in single measurement cycles. We investigate the influence of calculating a synthetic regenerative signal (sR) for SGC fitting, to reduce the effect of outliers on individual grain measurements. Furthermore, we reduced the regenerative cycles (rc) used for our sR approach, to test if shorter protocols would result in equivalent dose (D_e) estimates in agreement with longer protocols. We then calculated Spearman rank correlations between the results obtained with our modified SGC and the SAR protocol, luminescence signal intensities, and the geochemical dataset.

Finally, we present a new method of fitting data onto a SGC which significantly decreases measurement time, without risking the inclusion of outliers. We furthermore show that the luminescence signal intensities, the D_e values and their dose recovery ratios obtained with our SGC method and a SAR protocol, are independent of the sample geochemistry.

1. Introduction

In the recent past the interrelationship of life and the evolution of Earth's surface has been subject to intensified research activities (e.g., Amundson et al., 2007; Starke et al., 2020). The outermost shell of our planet, in which rocks, soils, water, air and biota interact and thus where this interrelationship takes place, is often referred to as the Earth's Critical Zone (ECZ) (Giardino and Houser, 2015). The Atacama Desert in Chile, generally considered the driest non-polar Desert on Earth, is an ideal study site to explore the dynamics of the water and biota free endmember of ECZ systems (e.g., Dietrich and Perron, 2006; Oeser et al., 2018; Tchakerian and Pease, 2015).

Single-grain luminescence dating has successfully been applied to infer sediment transport and mixing processes in the ECZ in various geological settings dissimilar to the Atacama Desert (Bonnet et al., 2019; Reimann et al., 2017; Román-Sánchez et al., 2019a,b). So far, optical stimulated luminescence (OSL) measurements carried out in the Atacama Desert were merely designed to determine the depositional age of sediments (e.g., Bartz et al., 2020a,b; Del Río et al., 2019; Diederich et al., 2020; May et al., 2020, 2015; Ritter et al., 2019; Veit et al., 2015) and dynamics inside a calcium sulphate wedge (Zinelabedin et al., 2022). Those studies revealed the unfavourable properties of Atacama Desert sediments especially regarding quartz OSL measurements. Quartz from the Atacama Desert has been shown to have a very low OSL sensitivity and unstable signal components (Bartz et al., 2020a; Del Río et al., 2019; May et al., 2015; Veit et al., 2015). Furthermore, a previous study on the applicability of luminescence dating of coarse grain feldspars from the Atacama Desert found highly variable potassium (K) contents within each sample and merely ~ 1 % of the measured feldspar grains gave a post-infrared infrared stimulated luminescence (pIRIR) signal suitable for dating (Zinelabedin et al., 2022). The heterogeneity of K-contents in feldspars poses a challenge in calculating internal dose rates and raises the question of whether the chemical composition of feldspars is related to luminescence properties.

Problematic quartz OSL properties have been reported previously and have been associated with the quartz source area (e.g., Bartz et al., 2020a; Sawakuchi et al., 2011; Tokuyasu et al., 2010), the depositional context of the sample (e.g., Fitzsimmons et al., 2010; Li and Wintle, 1992) or too few reworking cycles (e.g., Sawakuchi et al., 2011; Steffen et al., 2009). In some cases, coping strategies have been developed (Fuchs and Owen, 2008, Sawakuchi et al., 2011). So far, due to its unfavourable OSL properties, quartz has been discarded for luminescence dating of Atacama Desert sediments (e.g. Bartz et al., 2020a; Zinelabedin et al., 2022). Considerably fewer studies have addressed problematic

feldspars. Single-grain measurements of feldspars can be challenging and time-consuming, particularly when only a small percentage of grains emits suitable luminescence signals (e.g. Brill et al., 2018; O'Gorman et al., 2021; Sontag-González et al., 2021; Zinelabedin et al., 2022). In such cases many SG discs have to be measured before a sufficient number of grains has been obtained to calculate a robust palaeodose. This can result in such samples not being investigated further (Brill et al., 2018). Establishing a standardised growth curve (SGC) for single-grain feldspar pIRIR measurements reduces the measurement time considerably (Li et al., 2018). Sontag-González et al. (2021) showed that SGCs are also suitable for feldspars with unfavourable luminescence properties and a complex mineralogy.

Atacama Desert feldspars studied so far show highly variable K-contents with on average low K-concentrations (Zinelabedin et al., 2022). It is generally considered that a feldspar grain giving a luminescence signal has a K-content in the range of 8 to 13 % (12.5 ± 0.5 % Huntley and Baril, 1997 or 10 ± 2 % Smedley et al., 2012). Furthermore, Prescott and Fox (1993) (thermoluminescence) and Spooner (1992) (infrared stimulated luminescence) presented data for the whole composition range of the feldspar mineral group, showing a positive correlation of K-contents and signal intensity. In contrary, O'Gorman et al. (2021) and Zinelabedin et al. (2022) not only showed that grains with lower K-concentrations may emit suitable pIRIR signals but also that the majority of grains in a sample, which are used for D_e calculations, may have K-contents much below the proposed literature values (< 3 % and 3.9 ± 1 % respectively). Moreover Smedley et al. (2012) found no correlation between K-content and signal intensity on a single-grain level. In agreement with that Finch and Klein (1999) as well as Riedesel et al. (2021) propose a different source for signal intensity levels in the blue emission by linking them to Al-O-Al bridges, whereas Garcia-Guinea et al. (1999) connected signal intensity to alkali ion leakages caused by prolonged heating. This raises the question of whether, in the case of Atacama Desert feldspars, SG K-contents have to be determined for dose rate calculation and if correlations exist between the chemical composition of the feldspars and their luminescence properties.

In this study we aim to establish a methodological framework for time efficient single-grain luminescence-based analysis of feldspar samples from the Atacama Desert. We use a test dataset consisting of ten samples, five from the Atacama Desert and five chemically and structurally different feldspar sediment extracts from various geological origins from around the world. A dose recovery test ($pIRIR_{175}$) is performed on 500 grains per sample and the geochemistry of 300 out of the 500 grains is determined by using a scanning electron microscope (SEM) equipped with an energy-dispersive X-ray spectrometer (EDX). With this dataset we test the applicability of SGCs for single-grain pIRIR equivalent dose (D_e) determination of Atacama Desert feldspars, in order to reduce our measurement times and we use Spearman rank correlations to investigate the influence of geochemistry on luminescence properties and SGC performance.

2. Samples and instrumentation

2.1 Samples

Our sample suit consists of ten samples of different origin and chemical composition. Five samples (ARO-18-08-LP, CSA-1-2-2, LAGU-1-1, PAG-6-4b, PAG-6-6b) originate from the Atacama Desert. The remaining five samples originate from badlands in Canada (ABLR-1), lake sediments in Japan (HAM-5), a beach ridge in Chile ~ 1000 km south of the Atacama Desert (ISM-7), the Continental Deep Drilling (KTB) borehole in Germany (KTB-383-C) and the Mont-Blanc tunnel in Italy (MBT-I-2430). We chose the non-Atacama samples to reflect a range of chemical and structural variations of feldspar. Basic information on the samples are summarised in Table 1.

118 *Table 1: Sample description.*

Sample ID	Origin and subset affiliation	Coordinates		Grain size [µm]	Grain hole size [µm]	References
ARO-18-08 LP	Atacama Desert, Chile (A)	19°39'34.02" S	69°35'51.4" W	200 – 250	300	Zinelabedin et al., 2022
CSA-1-2-2	Atacama Desert, Chile (A)	19°36'20.17" S	70°5'52.12" W	100 – 200	200	-
LAGU-1-1	Atacama Desert, Chile (A)	21°1'59.37" S	69°47'53.00" W	100 – 250	300	-
PAG-6-4b	Atacama Desert, Chile (A)	21°32'31.7" S	69°54'47.9" W	100 – 200	250	Ritter et al., 2019
PAG-6-6b	Atacama Desert, Chile (A)	21°32'31.7" S	69°54'47.9" W	100 – 200	250	Ritter et al., 2019
ABLR-1	Badlands, Canada (X)	50°1'30.6" N	104°59'15.81" W	100 – 200	250	-
HAM-5	Lake Hamana, Japan (X)	34°45'8.65" N	137°34'22.62" E	100 – 200	250	Riedesel et al., 2021, 2019
ISM-7	Beach ridge, Chile (X)	37°1'20.28" S	73°30'43.49" W	100 – 200	250	-
KTB-383-C	KTB Borehole, Germany (X)	49°48'55" N	12°7'14" W	180 – 250	250	Guralnik et al., 2015
MBT-I-2430	Mount Blanc Tunnel, Italy (X)	45°50’07’’ N	6°55’59’’E	180 – 212	250	Lambert, 2018

119

Prior to luminescence measurements the samples were sieved and treated with HCl (10 %), H_2O_2 (10 %) and $Na_2C_2O_4$ (0.01 N), to remove carbonates and organics and to disperse the particles, respectively. Subsequently, samples were sieved again to obtain different grain size fractions (Table 1). A heavy liquid density separation was used to enrich the K-rich feldspar proportion ($\rho < 2.58$ g/cm³). Sample KTB-383-C feldspars were etched with HF afterwards.

2.2 Luminescence

For the dose recovery tests the samples were loaded into standard single-grain discs under a microscope under daylight conditions, for grain hole sizes used see Table 1. A single hair was used to ensure that all 100 holes per disc were filled with one grain each. Despite this, for the samples CSA-1-2-2, HAM-5 and KTB-383-C it was sometimes unavoidable to have several grains in one hole. Prior to the dose recovery test, all mounted grains were bleached in a SOL2 solar simulator for 24 h.

An automated Risø TL/OSL reader (DA-20) equipped with a $^{90}Sr/^{90}Y$ beta source for irradiation, delivering a dose rate of ~0.08 Gy/s, was used for all luminescence measurements. A 150 mW 830 nm centred IR laser stimulated the grains, and the blue (~410 nm) was detected through a combination of two 2 mm Schott BG-39 filters and a 3 mm Corning 7-59 glass filter. A dose-rate map (Lapp et al., 2012), created by using radiosensitive film (GAF), showed a dose uniformity across the sample area of ~4.5 %. It is thus not expected to significantly contribute to the received doses of each grain. A dose recovery test (DRT, given dose = 150 Gy) was carried out employing a pIRIR protocol (Thomsen et al., 2008) with a preheat of 200 °C for 60 s and a pIRIR stimulation temperature of 175 °C. The IR_{50} and $pIRIR_{175}$ measurement times were 2 s and 3 s, respectively. For further details on the single-aliquot regenerative-dose (SAR) DRT protocol used see Table 2.

Table 2: Single-grain dose recovery test SAR measurement protocol. Heating rate for steps 2-4 and 6-8 2 °C/s.

Step	Treatment[a]	Observation
1	Given dose D_i	
2	Preheat, 60s at 200°C	
3	IRSL, 2s at 50°C	
4	IRSL, 3s at 175°C	L_x
5	Given test dose D_t	
6	Preheat, 60s at 200°C	
7	IRSL, 2s at 50°C	
8	IRSL, 3s at 175°C	T_x
9	Return to step 1	

[a] given dose D_i [Gy]: 150, 0, 50, 150, 300, 500, 800, 0, 50, 150; test dose Dt [Gy]: 50

For signal integration the first 0.2 s minus a background of the last 0.4 s of stimulation was used. Five discs à 100 grains were measured per sample.

All D_e estimates and SGCs were derived using the numOSL R package (Peng et al., 2018) and the least-squares (LS)-normalisation approach following Li et al. (2016). A measurement error for the regenerative dose signal (L_x) and the corresponding test dose signal (T_x) of 2 % was used for calculations. Parameters used for growth curve fitting were: “exponential model”, “not forced through

origin" and "using a weighted procedure". Rejection criteria for the SAR and SGC approaches were as follows: test dose signal following natural dose measurement (T_n) > 3 sigma above background, relative standard error (RSE) of $T_n \leq 25$ %, recycling ratio = unity ± 10 %, recuperation ≤ 10 % of the natural signal, recuperation ≤ 10 % of the maximum regenerative-dose signal, figure-of-merits (FOM) ≤ 10 % (Peng and Li, 2017), reduced chi square ≤ 10 %. The FOM, a measure of goodness-of-fit, is calculated as follows: FOM = $\sum|y_i^o - y_i^f|/\sum y_i^f * 100$ (Balian and Eddy, 1977). D_e with a RSE above 50 % were rejected after their calculation. A dose value of 150 Gy was used for SAR dataset re-normalisation in the pickSARdata() function.

2.3 Geochemistry (SEM-EDX)

Following the luminescence measurements double-sided sticky tape, on one side attached to a glass microscope slide, was placed on the top side of the SG discs. The undersides of the SG discs were lightly tapped with a piezoelectric ultrasonic cleaner (vibration frequency 30 ± 3 kHz) to transfer the grains onto the tape. About 80 % of the grains were extracted on average. Prior to disc removal from the tape the location of the disc position holes was marked on the tape. Subsequently the grains were embedded in colourless two-component epoxy resin (Araldit 2020, Huntsman), with position hole placement marked on the epoxy discs. The surfaces of the epoxy discs were sanded with a 1200 SiO_2 sandpaper and polished to ensure that no epoxy covers the grains.

The chemical composition of individual grains was determined on a Zeiss Sigma 300-VP scanning electron microscope (SEM) with an energy dispersive spectroscopy (EDX) attachment. The working distance was set to 8.5 mm. The aperture diameter of 60 µm and an accelerating voltage of 20 kV resulted in an output count rate of ~ 45,000 cps. The chemical composition of individual feldspar grains was calculated based on the nine elements O, Na, Mg, Al, Si, K, Ca, Ti and Fe through stoichiometry. Three out of five discs per sample were measured for their geochemical composition. For the samples ISM-7, LAGU-1-1 and MBT-I-2430 two discs were analysed.

2.4 Statistic

For data comparison Spearman rank correlations were used (Spearman, 1904). The results of a Spearman rank correlation, the Spearman's rank correlation coefficient (r_s), can range between -1 and 1, with -1 being a perfect negative correlation and 1 a perfect positive correlation. The closer the r_s value is to zero, the weaker the correlation. We here define correlations with r_s values between 0 and ± 0.2 as very weak, between ± 0.2 and ± 0.4 weak, between ± 0.4 and ± 0.6 moderate, between ± 0.6 and ± 0.8 moderate to strong and between ± 0.8 and ± 1 strong. The significance of a correlation was tested using the cor.mtest() function of the corrplot() package (Wei and Simko, 2023). This test results in p-values for each correlation pair. If the p-value is > 0.05, the correlation is not significant.

All errors given here for D_e values correspond to one standard deviation. Presented arithmetic means are always given with the corresponding standard error.

3. Standardised growth curve (SGC) application and modification

3.1 SAR and SGC

3.1.1 Procedure

To test the applicability of the SGC approach, first the dose response properties using the standard SAR approach were assessed. For further analysis the dataset was divided into two subsets, Atacama Desert (A) and external (X) samples (cf. Table 1). For each subset A and X one SGC was calculated using the numOSL R package and the above-mentioned rejection criteria. Since the Atacama Desert samples are of main interest for this research, the SGC for subset A is hereafter called SGC. The SGC for subset X is referred to as xSGC and not used for direct comparison between SAR and SGC D_e values of dataset X. The xSGC will be used in following sections for D_e calculation of grains from dataset A (see Fig. 1). Following Li et al. (2015a) two SAR cycles are needed for the D_e calculation using an existing SGC. Besides the "natural" cycle (L_n/T_n), an additional regenerative cycle with a regenerative dose D_{r1}, and test dose signal L_{r1} and T_{r1} is required for the projection onto the existing SGC. According to Li et al. (2015a) the size of D_{r1} should be close to the expected size of the D_e. Our expected dose is 150 Gy, which equals the regenerative dose of regenerative cycle R3 or R9. Unfortunately, the L_x/T_x values of regenerative cycle R3 and R9 often showed large deviations from the fitted growth curves of up to 44 % (see Fig. 2). Consequently, we decided to use regenerative cycle R2 (50 Gy) as D_{r1}.

3.1.2 Results & discussion

When using the standard SAR approach 657 grains out of 5000 analysed grains (13.1 %) passed the rejection criteria and resulted in a D_e. Most of the grains (56.7 %) were rejected due to T_n signals below 3 σ above background. Another 15.6 % were rejected based on poorly-fitted growth curves and 11.6 % were rejected for a T_n with a RSE > 25 %. For details on rejected grains see supplement Table S1. Three additional grains were rejected due to their D_e value having a RSE > 50 %. The mean of the remaining 654 D_e values was 128 ± 36.1 Gy, which corresponds to a dose recovery ratio (DRR) of 0.85 ± 0.01. MBT-I-2430 was the sample giving the most D_e values (309 grains ≈ 47.2 %) and PAG-6-4b the one with the least (1 grain = 0.15 %).

From the Atacama Desert samples (subset A) merely 88 out of 2500 grains were accepted resulting in 87 D_e. Whereas from the external samples (subset X) 569 out of 2500 grains were accepted resulting in 567 D_e values. In each subset one sample was dominating the following results. In subset A grains from sample LAGU-1-1 make up 71.3 % of the total number of accepted grains. While in subset X 54.5 % of the accepted grains were from sample MBT-I-2430. The DRR of 0.89 ± 0.02 for subset A was slightly better than for subset X with a DRR of 0.85 ± 0.01.

The Atacama Desert samples are of main interest for this research, thus only D_e calculations for subset A are discussed in the following sections. Since the rejection criteria for the SAR and SGC methods were the same, 88 grains from subset A were used for the SGC construction and subsequent D_e calculation using the constructed SGCs. The goodness-of-fit of the SGC can be evaluated using the FOM. Peng and Li (2017) recommended a FOM below 10 % for SGCs. Before the LS-normalisation the FOM of the SGC was 16.4 %. The LS-normalisation reduced the scatter between the grains in dataset A which lead to a FOM value of 10.1 %, slightly above the recommended 10 %. The D_e calculation with the SGC was possible for 87 out of 88 grains. The DRR of the remaining SGC-acquired D_e values was 0.84 ± 0.03.

In previous papers the agreement of SAR and SGC results was based on their D_e values ± their 2 σ standard error (e.g., Li et al., 2015a,b; Sontag-González et al., 2021). When reporting luminescence ages the 1 σ standard error is commonly used (Mahan et al., 2022). The D_e values had average RSEs of ~16 %, therefore the agreement within 1 σ seems inappropriate to evaluate the differences between the SAR procedure and the SGC method. Therefore, we focus on the number of grains differing less than ± 10 % in their calculated D_e values (Fig. 1A) and on Spearman rank correlations.
For 86 grains D_e values were calculated with both methods and were used for the comparison. Of those 86, 41 D_e values did not differ more than ± 10 %, 37 additional had indistinguishable D_e values at 1 σ and 8 additional in 2 σ. SAR and SGC results correlate with a r_s of 0.81, which can be regarded as the lower limit of a strong correlation.

There are several reasons why the D_e values of a grain calculated with the two different methods might not agree within ± 10 %. Firstly, the dataset for constructing the SGC is very small (n = 88). Secondly, the fit of the SGC is not considered good due to the FOM > 10 % (Peng and Li, 2017). Thirdly, even though D_{r1} was chosen to reduce the influence of outliers, some L_{r1}/T_{r1} still showed deviation from the growth curve of up to 35 %. Fourthly the overall large RSE of the dataset indicates poor luminescence properties.

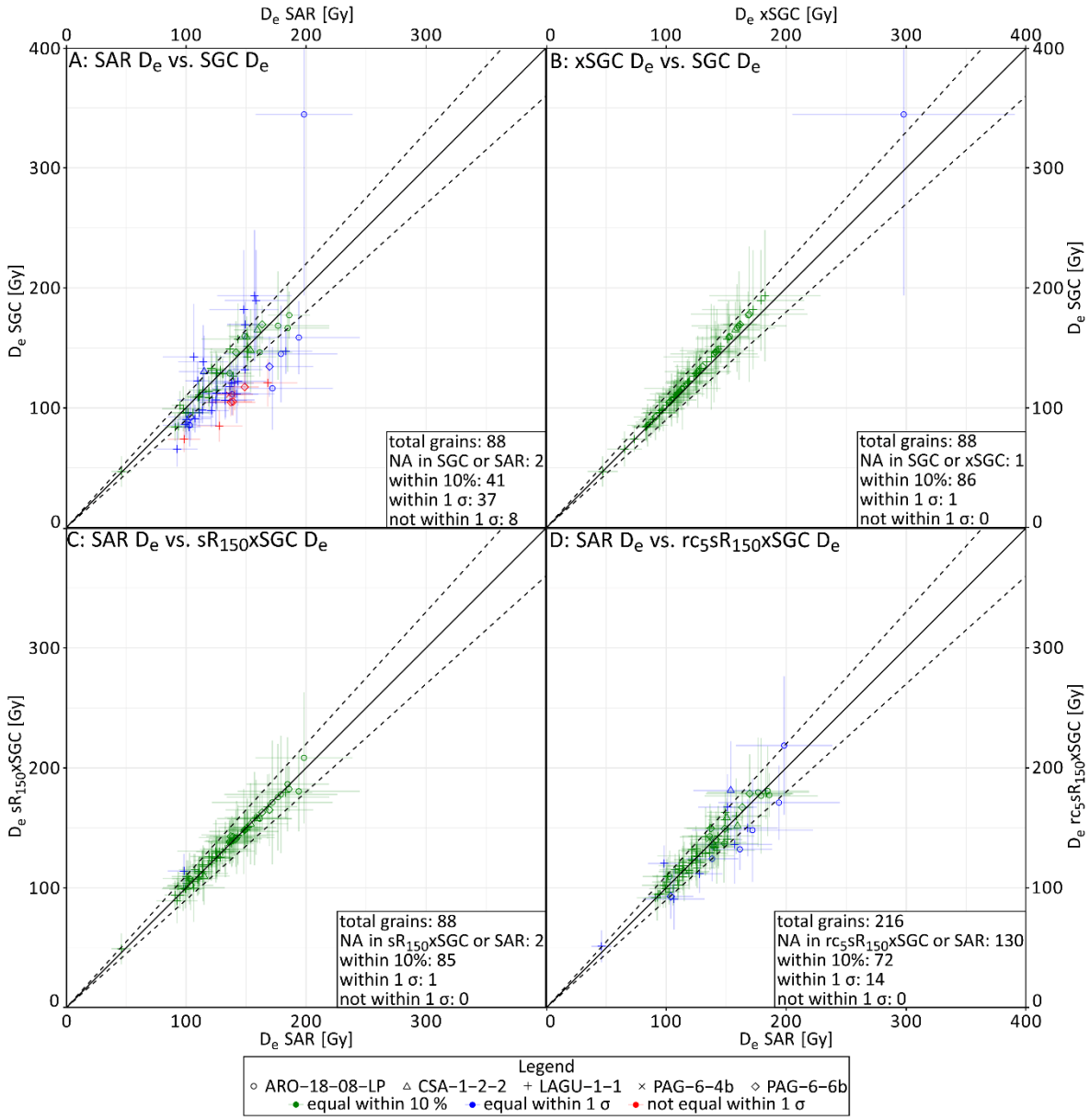

Fig. 1: evaluation of SGC performance. ***A)*** *comparison of D_e from samples of dataset A (Table 1) obtained by the standard SAR procedure with D_e obtained using a SGC established with the same measurements, fitted with their L_{r1}/T_{ri} from the third SAR cycle with a D_{r1} of 50 Gy (Table 2);* ***B)*** *comparison of D_e from samples of dataset A obtained by a SGC, established using the same samples, and obtained by a xSGC, constructed with data from subset X (Table 1);* ***C)*** *comparison of D_e from samples of subset A obtained by the standard SAR procedure with D_e obtained using the xSGC from B) and fitting the individual grains with L_{sR}/T_{sR} from an synthetic cycle with a D_{r1} of 150 Gy (sR_{150}xSGC);* ***D)*** *comparison of D_e from samples of subset A obtained by the standard SAR procedure with D_e obtained using the sR_{150}xSGC from C) and reducing the SAR-cycles for individual growth curve fitting to the "natural" 150, 0, 50, 500, 50 Gy cycles (rc_6sR_{150}xSGC).*

3.2 External SGC (xSGC)

3.2.1 Procedure

In future studies it seems more likely to use an already established SGC than constructing a SGC for every new sample side. Therefore, the established SGC might be constructed from samples with different geographical and geological origin than the samples it is used for. To mimic this scenario, we test the performance of the xSGC, build with subset X, to analyse subset A. The xSGC was constructed

in the same manner as the SGC (see section 3.1.1). For the subsequent D_e calculation of dataset A the parameters of the xSGC were used in the calSGCED() function.

3.2.2 Results & discussion

Next the D_e results using the SGC and xSGC are compared in the same manner as SAR and SGC above (Fig. 1B). Using the xSGC, D_e values for all 88 grains could be calculated. A total of 87 mutual grains were used for the comparison between SGC and xSGC. All but one of them agreed within less than ± 10 %. If the SGC D_e is considered to be the true D_e, xSGC D_es all slightly underestimated with an average of 4.14 ± 0.56 Gy. The large uncertainty is caused by one grain not being within ± 10 % in unity. The correlation between both D_e results is perfect with a r_s of 1.

The one grain, which differed slightly more than 10 %, is still in agreement if the 1 σ errors of the two D_e values are considered (cf. Fig. 1B). This particular grain had an outlier in its L_x of the second regenerative cycle (R2) with an unusual low net signal and a relatively high background. SGC and xSGC calculated unusually high D_e values based on this one L_x/T_x. With D_e values of 345 ± 150.8 Gy for the SGC and 298 ± 92.7 Gy for the xSGC, they were around twice as high as the given dose of 150 Gy. For comparison the SAR D_e for this particular grain was 198 ± 40.3 Gy, which demonstrates that outliers in individual measurement cycles can have a considerable effect on the SGC results if the outliers occur in the D_{r1} cycle.

In general, the deviation between D_e derived with the different SGCs increases with increasing L_n/T_n. As with the D_e calculation using a SAR growth curve, small changes in L_n/T_n result in larger changes in the D_e the closer to saturation they intersect the growth curve. L_n/T_n above $2D_0$ are therefore usually not considered (Murray et al., 2002).

The agreement between SGC and xSGC results confirms Li et al. (2015b) findings, that a 'global SGC' is suitable for feldspar samples and Mueller and Preusser (2022) observations that SGC results are not biased if the same input grains are used for SGC construction and application.

In our future studies in the Atacama and elsewhere, the case of using a xSGC seems more likely because it is created with a larger dataset and might thus be more robust. Since the correlation between SGC and xSGC D_e values is perfect, all further data is generated with the xSGC.

3.3 Synthetic R (sR)

3.3.1 Procedure

When fitting a SAR growth curve using any function, in our case a single saturating exponential, all L_x/T_x points measured are taken into account by the fit. However, when interpolating data onto a constructed SGC only the natural signal and one regenerative dose point is used (Li et al., 2015a), however, as mentioned in section 3.2.2 this can lead to erroneous results, should this value deviate significantly from the fitted growth curve (cf. Fig. 2). Here we introduce a new parameter and procedure for the projection of multiple L_x/T_x onto the constructed SGC. Instead of using a single L_x/T_x point as

L_{r1}/T_{r1} we chose a L_x/T_x point, which we extracted from the fitted growth curve. We term this point synthetic regenerative dose (sR). For this we used the growth curves of each grain and reversed the process of D_e estimation from a growth curve. We chose an sR, for example 200 Gy (cf. Fig. 2), and inserted it into our exponential function (eq. 1). Thereby we projected the sR onto the growth curve whereby we calculated the point of interception with the growth curve to get the value on the y-axis of our synthetic L_{sR}/T_{sR} (Fig. 2).

$$\text{(eq. 1)} \quad \frac{L_{sR}}{T_{sR}} = a * \left(1 - exp^{(-sR*b)}\right) + c$$

With a, b and c being the parameters a, b and c from the grain-wise exponential growth curve, calculated during the normal SAR procedure and sR a value in Gy.

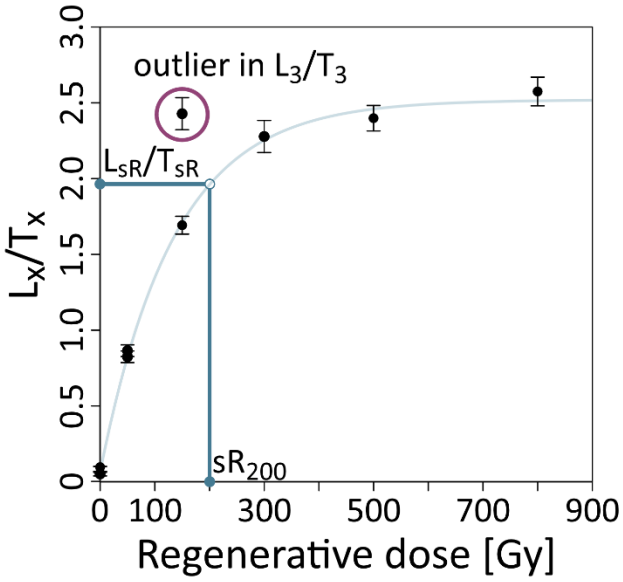

Fig. 2: Process of L_{sR}/T_{sR} determination with an sR of 200 Gy on an example exponential SG growth curve with an outlier in the L_x/T_x of the third regenerative SAR cycle (D_i = 150 Gy). The vertical line from the X-axes towards the growth curve illustrate the process of calculating the interception. The horizontal line from the growth curve towards the Y-axes illustrate the subsequent determination of L_{sR}/T_{sR}.

To evaluate if there is an influence of the size of sR on the resulting D_e and DRR we tested eight different sR values: sR_{50}, sR_{100}, sR_{125}, sR_{150}, sR_{175}, sR_{200}, sR_{300} and sR_{800}, with the subscript being the size in Gy.

3.3.2 Results & discussion

The results were evaluated in the same manner as SAR and SGC in section 3.1.1 based on a comparison of D_e and DRR results of the SAR procedure and the $sR_{50\text{-}800}$xSGC procedures. For detailed results of all sR tested see supplement Table S2). For all sR sizes, except for 800 Gy, 86 D_e values for the 88 not rejected grains were calculated. With sR_{800} 87 D_e values were calculated. Since sR_{100}, sR_{125} and sR_{150} had the most grains within 10 % in unity with the SAR results, the other five sR values will not be discussed further. With sR_{125} all grains had D_e values within 10 % in unity with the SAR D_e values, whereas sR_{150} had one and sR_{100} three grains not within 10 %. With DRRs of 0.86 ±0.02, 0.87 ±0.02 and

0.89 ±0.02 for sR_{100}, sR_{125} and sR_{150} respectively all three sR procedures showed an improved DRR compared to the above presented conventional SGC approach (0.84 ±0.03). The correlation between the SAR D_e values and those achieved with sR_{100}, sR_{125} and sR_{150} was strong positive with Spearman's rank correlation coefficient (r_s) of 0.99 for all three sR values tested. The differences between sR_{100}, sR_{125} and sR_{150} were small, with sR_{125} having the most D_e results equal within 10 % with the SAR procedure but sR_{150} yielding the better DRRs.

Deviations of sR from the expected D_e (here 150 Gy) of ~ 30 % (± 50 Gy), do not cause major alterations in the D_e results in this data set. All sR ranging from 100 to 200 Gy have a strong positive correlation with the SAR procedure, with a minimum r_s of 0.94. In comparison with the SAR data, if the sR was slightly smaller than the expected D_e ($sR_{100,125}$), the method yielded better results than if the sR was slightly larger ($sR_{175,200}$). A cause for the better agreement with the SAR results might be the overall underestimation of the D_e with the SAR procedure. Since the differences between the best performing sR were very small and the sR_{150} had the same DRR as the SAR procedure, we chose an sR of 150 Gy for our further analysis (see Fig. 1C). Furthermore, the sR_{150} equals the recommended size for a D_{r1}(Li et al., 2015a). We therefore conclude that sR should be chosen to be the same size as the expected D_e. Nevertheless, considering that the D_e is normally unknown before measurement, it is reassuring that choosing an sR value within 30 % of the natural dose does not seem to have too great of an effect on final De calculations.

3.4 Reduction of SAR cycles (rc)

3.4.1 Procedure

Whilst the sR approach helps in making the interpolation onto the SGC more robust, it still requires the construction of a full growth curve for every grain and thus not saving any measurement time. Here we test which cycles can be removed to save time while still yielding robust D_e values with the sR_{150}xSGC method. We carried out ten different reduced cycle (rc) scenarios, all containing the "natural" cycle and a zero-dose cycle (recuperation). Besides these two cycles, we tested if two additional cycles are enough to incorporate the sR method or if a third cycle, a recycling point, is needed as well. We also investigated which dose size yielded the best results. For the recycling point we could only test 50 Gy and 150 Gy since those were the only recycling doses in our SAR protocol. The ten tested rc scenarios are listed in Table 3 and afterwards abbreviated with their test number according to Table 3 as a subscript. The dataset used for xSGC calculation was not reduced.

Table 3: reduced cycle scenarios tested for subset A. For all cycles measured see Table 2.

Abbreviation	Used cycles	D_i of used cycles [Gy]
rc_1	N + R1 + R2 + R4	150 + 0 + 50 + 300
rc_2	N + R1 + R2 + R5	150 + 0 + 50 + 500
rc_3	N + R1 + R2 + R6	150 + 0 + 50 + 800
rc_4	N + R1 + R2 + R3 + R8	150 + 0 + 50 + 150 + 50
rc_5	N + R1 + R2 + R4 + R8	150 + 0 + 50 + 300 + 50
rc_6	N + R1 + R2 + R5 + R8	150 + 0 + 50 + 500 + 50
rc_7	N + R1 + R2 + R6 + R8	150 + 0 + 50 + 800 + 50
rc_8	N + R1 + R3 + R4 + R9	150 + 0 + 150 + 300 + 150
rc_9	N + R1 + R3 + R5 + R9	150 + 0 + 150 + 500 + 150
rc_{10}	N + R1 + R3 + R6 + R9	150 + 0 + 150 + 800 + 150

3.4.2 Results & discussion

The reduction of used SAR cycles led to an increase of accepted grains. Fewer grains were rejected due to poor growth curve fitting. For detailed rejection criteria and results of all tested rc see supplement Table S3 and S4.

The growth curves produced in rc_4 used for the sR method are not reliable since the highest given dose used for their calculation is still in the linear part of the growth curves constructed with the full set of SAR cycles. Many grains were falsely excluded as they appeared to be saturated. Furthermore, the results did not agree well with the SAR procedure and a poor DRR was obtained (see Table S4), thus rc_4 is not discussed further. All other tested rc were able to calculate ~ 200 D_e values out of the 2500 measured grains.

In a direct comparison to the SAR D_e values, all ten tested rc had at least 85 common grains with the SAR results. Rc_5 had the most D_e values equal with the SAR D_e within ± 10 % and no D_e not within 1 σ. Rc_1, rc_2 and rc_6 performed slightly worse, but their D_e values also did not differ more than 1 σ. The remaining six rc had at least one grain, which was not within 1 σ of the SAR results and are therefore not discussed further. Since the Spearman's rank correlation coefficients between rc-achieved D_e values and those calculated with the SAR procedure for rc_1 and rc_2 were below the r_s of 0.94 from rc_5 and rc_6, we concentrate on the latter two.

Rc_5 and rc_6 had the same setup for the cycle reduction, with remaining cycles being the “natural” cycle, a zero-dose cycle, a recovery dose of 50 Gy plus one additional dose. The additional doses of 300 and 500 Gy, respectively, are between D_0 (284 Gy) and $2D_0$ (568 Gy) of the xSGC. Rc_6 was able to calculate eight D_e more than rc_5 but rc_5 had the best overall results. With rc_5 197 D_e values were calculated, of which 72 were equal with the SAR results within ± 10 % and the remaining 14 D_e were identical within

the 1 σ error (cf. Fig. 1D). The mean difference between the D_e values was 7.40 ± 0.70 Gy and the DRR of rc_5 was 0.9 ± 0.02, which is slightly better than the SAR-achieved DRR of 0.89 ± 0.02.

Compared to the correlation of the sR_{150}xSGC results, with a r_s of 0.99, the correlation of the rc_5sR_{150}xSGC and the SAR approach is worse with a r_s of 0.94. Nevertheless, the rc_5sR_{150}xSGC is still an improvement compared to the conventional SGC approach (r_s = 0.81, DRR = 0.84 ± 0.03). Furthermore, it is possible to estimate more than twice as many D_e, resulting in fewer discs to be measured. The reduction of measurement cycles saves approximately 60 % of measurement time per disc.

We therefore recommend applying the rcsRxSGC approach when dealing with problematic single grain feldspars, with an sR in the size of the expected D_e and a rc scenario with a recuperation point, a recycling point - smaller than the expected D_e, and an additional dose point with a size of D_0 to $2D_0$ of the SGC used.

3.5 Dose recovery ratio (DRR)

Since our dataset is based on a dose recovery test, another measure to test the performance of our approach is the dose recovery ratio. Overall the given dose of 150 Gy is underestimated by all applied methods, including the standard SAR procedure. Fig. 3 shows a comparison of the D_e results achieved with the SAR procedure and the rc_5sR_{150}xSGC method. With the SAR procedure, 30 out of 87 grains yield a DRR within the desired 1 ± 0.1. An additional 22 were still within 1 ± 0.1 if their 1 σ errors were considered and 35 differed more than ± 0.1 from a DRR of 1 even when their 1 σ errors were considered. Out of the 216 calculated D_e with the rc_5sR_{150}xSGC method, 54 had a DRR of 1 ± 0.1. An additional 80 were still within 1 ± 0.1 if their 1 σ errors were considered and 82 differed more than ± 0.1 from a DRR of 1 even when their 1 σ errors were considered. Thus, using the rc_5sR_{150}xSGC method we observed overall improved DRR.

The generally observed underestimation of the given dose could be due to the protocol not being suitable for all samples, or due to fading of the pIRIR signals. We also considered changes in sensitivity during the first measurement cycle (see Kars et al., 2014), but we could not find any indication for this (data not shown).

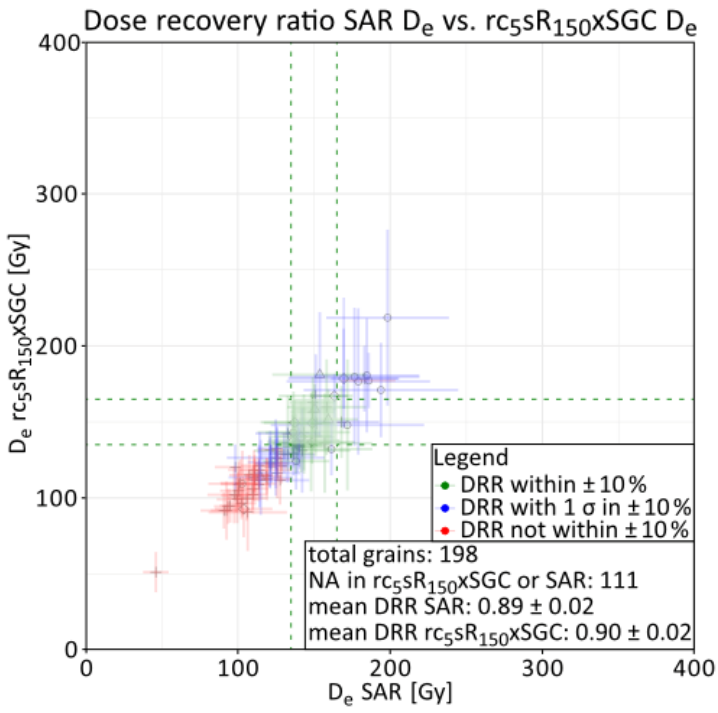

Fig.: 3: DRR from grains of subset A, calculated with the standard SAR procedure (x-axes) and the rc5sR150xSGC method (y-axes). Colours of the horizontal and vertical 1 σ error bars represent if the DRR calculated with SAR or rc5sR150xSGC respectively are within 1 ± 10 % (green), within 1 ± 10 % if the 1 σ error is considered (blue) or if they are not within 1 ± 10 %. Shape of the datapoints indicate the sample allocation (cf. legend Fig. 2).

4. Single grain geochemistry (SEM-EDX)

4.1 Procedure

The SEM-EDX measurements were carried out at the Institute of Geology and Mineralogy of the University of Cologne, by defining regions of interests on the grain surfaces. The elemental analysis results of each measured region were assigned to the individual grains on the basis of the tomograms of the measurements.

Unfortunately, SEM-EDX data could not be obtained for every grain. Some grains got lost during the transfer process from the discs to the tape, the position of others was slightly altered during embedding them in epoxy. If a grain was subsequently not clearly identifiable, its SEM-EDX results were not considered. For some grain positions (i.e., holes in the discs) more than one SEM-EDX result was obtained. This was either due to multiple grains being located in one hole or due to breaking of the grains during the transfer process. For grains and holes with more than one SEM-EDX measurement result, the average was calculated.

4.2 Results

The results for the nine analysed elements are summarised in Fig. 4, for detailed measurement results see supplement Table S5. 2328 grains, out of the 5000 grains analysed for their luminescence

characteristics, could be clearly identified on the SEM-EDX tomograms. From those 2328 grains, 250 gave suitable luminescence signals for D_e calculation with the SAR procedure and 492 with the $rc_5sR_{150}xSGC$ method. Those grains are hereafter called luminescent grains. All luminescent grains from subset A (n = 65) contained O, Na, Al, Si and K, implying that no luminescent grain from the Atacama Desert was pure orthoclase. About half of them also contained Ca and Fe. From subset X (n = 434) most of the grains (>400) were also composed of O, Na, Al, Si and K, with 200 of them also having Ca and 15 of them being pure orthoclase, based on their geochemical composition.

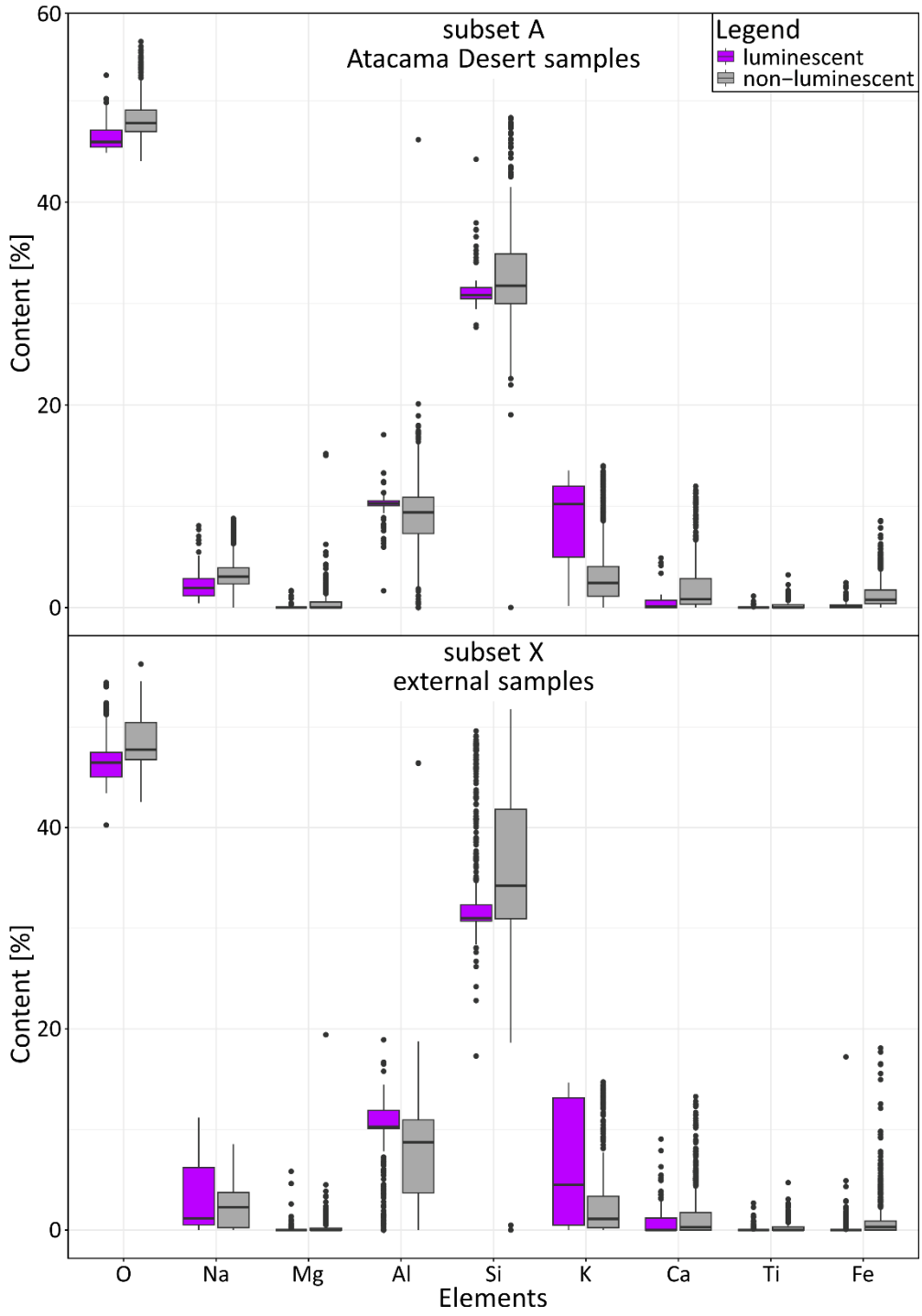

Figure 4: statistical distribution of all measured element concentrations for A) the grains from subset A and B) the grains from subset X grouped into luminescent (purple) and non-luminescent grains (gray).

The K-content of all luminescent grains varied between 0.06 wt% and 14.6 wt%, with a mean value of 7.04 ± 0.26 wt%. The coefficient of variation of all luminescent grains of 80 % indicates that luminescent grains can have a wide range of K-contents, supporting the findings from O'Gorman et al. (2021) and Zinelabedin et al. (2022).

The SEM-EDX results presented in Fig. 4 suggest that there is no clear difference between the

geochemical composition of luminescent and non-luminescent grains, neither for subset A nor subset X.

5. Correlation of luminescence characteristics and geochemistry

To evaluate whether signal intensity and K-content are linked and if there are further relationships within and between geochemistry and luminescence properties, we created the following nine correlation matrices. We performed Spearman rank correlations for the entire dataset and the two subsets. We then calculated six correlation matrices for these three categories by dividing them in luminescent and non-luminescent subgroups. In addition to the nine elements from the SEM-EDX analysis, the following luminescence properties were used as input variables: D_e and DRR determined with SAR, D_e and DRR determined by $rc_5sR_{150}xSGC$, L_n and T_n. For better readability, only the correlation matrix of the entire data set is shown in Fig. 5. The eight remaining correlation matrices can be found in supplement Fig. S1.

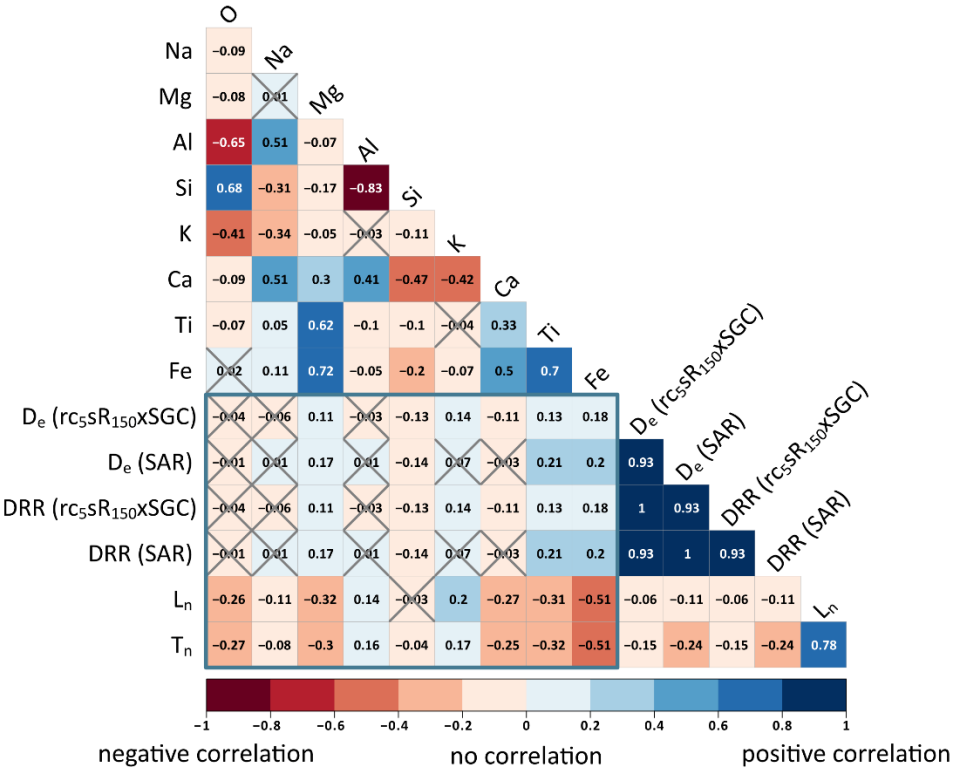

Fig. 5: correlation matrix of the complete dataset (subset A + X). Numbers in the squares represent Spearman's rank correlation coefficient values and their colour the strength of the correlation. For not significant correlations with a p-value above 0.05 % the squares are x-ed out. The turquoise square surrounds the correlation between the geochemical data and the luminescence characteristics.

There was no strong or moderate to strong correlation between any element and luminescence characteristics if the entire dataset is considered, as can be seen inside the blue square in Fig. 5. This also holds true regardless of whether the subset data or subgroups of the entire or subset data are considered. Furthermore, ~ 47 % of those correlations have a p-value > 0.05 and are therefore not

considered significant. The most significant correlation between SEM-EDX results and luminescence is the negative correlation observed between the Fe-content and the signal intensity (L_n and T_n) in the correlation matrix of all grains from subset X with a r_s of -0.57 and -0.56 for L_n and T_n respectively. The correlation between Fe-content and signal intensities in subset A is also negative but only very weak or weak, if significant at all. There is no significant correlation between K-content and the signal intensity (L_n and T_n) in subset A when only the luminescent grains are considered, but a weak negative correlation can be found in subset X. In contrast, the same correlation for the non-luminescent grains is very weak to weak positive in both datasets. In Fig. 5 these correlations between K-content and L_n respectively T_n are weak and very weak positive, since a greater number of non-luminescent grains contribute to the overall correlation in Fig. 5 (cf. Table S5). Conversely, Na and Ca contents show a positive correlation with the signal intensity in the luminescent grains and a negative correlation in the non-luminescent ones.

Within the luminescence characteristics there is no strong significant correlation between the signal intensity and the D_e or the DRR. Since the D_e values and DRRs determined with the same method have a perfect correlation, all correlations between D_es and DRRs determined with different methods yield the same r_s values within each correlation matrix. For subset A the r_s of these correlations is 0.94, for subset X and for both subsets combined it is 0.93. The correlation between L_n and T_n is almost perfectly positive if only the luminescent grains are considered, but substantially weaker if all or just non-luminescent grains are correlated.

Within the geochemical data the correlation values between the nine correlation matrices vary to a greater extent than within the luminescence characteristics. Correlations found between different elements reflect the general chemical characteristics of the feldspar mineral group, with Si:Al ratios differing between alkali feldspars and plagioclase and with a known miscibility gap between K- and Ca-feldspars. The strong negative correlation between Si and Al contents is particularly pronounced when only the non-luminescent grains are considered, but visible in all nine matrices. When only the luminescent grains are considered the correlations between K and Na as well as K and Ca contents are moderate to strong negative, while the correlations between Na and Ca contents are moderate or very strong positive. None of the K-, Na- and Ca-content correlations is more than moderate in the non-luminescent correlation matrices but all are in the same directions as in the luminescent grains.

The luminescent grains from sample ARO-18-08-LP have a very strong negative correlation of -0.83 and -0.86 between their Fe-contents and the signal intensities L_n and T_n. Zinelabedin et al. (2022), investigating the same samples, suspected that the high Fe-contents might be caused by Fe-rich coatings of the feldspar grains. These iron layers around the sediment grains could on the one hand explain the high Fe-content of up to 8.8 % in luminescent grains and on the other hand the observed low luminescence intensities, since Fe coatings could cause absorption of the emitted luminescence (Kook

et al., 2011). Geake et al. (1972) and Finch and Klein (1999) present alternative explanations for the negative correlation between Fe-content and L_n and T_n intensities. Ultimately, we cannot give a satisfactory explanation of the observed negative correlation between Fe-content and luminescence intensity at this stage.

The previously reported and generally accepted relationship of K-content and luminescence signal intensity is not supported by our data. The non-existing correlation between K-content and signal intensity in subset A confirms the findings of O'Gorman et al. (2021) and thereby falsifies the common hypothesis of a positive correlation (e.g., Huntley and Baril, 1997; Prescott and Fox, 1993; Spooner, 1992) at least for our set of samples. The weak negative correlation in subset X is further evidence that a higher K-content is not the main determinant for a high signal intensity.

6. Conclusion

Atacama Deserts feldspars are challenging for single grain luminescence measurements for two reasons: firstly, only a small percentage of grains emits satisfactory luminescence signals (Ø 3.52 %) and secondly their geochemical compositions are highly variable (Ø 3.40 wt% K).

To obtain a sufficient number of accepted grains for palaeodose calculation, numerous discs have to be measured, resulting in a long overall measurement time. We therefore tested the application of the standardised growth curve (SGC) method (Li et al., 2015b) with a dose recovery test using a $pIRIR_{175}$ protocol on ten chemically different feldspar sediment extracts. With a perfect correlation between SGC and xSGC results, we confirmed, that the geographical and geological origin of the samples, for which the D_e is estimated, can differ significantly from the geographical and geological origin of the samples used for SGC construction and that the SGC is not biased if the same input grains are used for SGC construction and application.

We introduced a new and more robust method for interpolation of L_x/T_x values onto the SGC. The new sR (synthetic regenerative dose) method, reduces the influence of outliers in individual L_x/T_x on the interpolation and D_e calculation. With the sR method a synthetic L_x/T_x, based on the growth curves of the individual grain, is used for D_e calculations with the SGC method. Since the sR method relies on the individual growth curves, no measurement time is saved. Therefore, we further tested how to reduce regenerative cycles (rc) to obtain a suitable growth curve for the sR method. With our new established rcsRxSGC method we were able to reduce our measurement time per disc by ~60 %. Furthermore, we were able to calculate around twice as many D_e per disc with the rcsRxSGC method than with the SAR procedure. Thus, potentially more measurement time can be saved, since fewer discs need to be measured to gain a sufficient amount of suitable grains.

We investigated the relationship of K-content and luminescence characteristics, as well as their implications for internal dose rate determination. Therefore, we measured the geochemical composition of the grains previously analysed for their luminescence properties using a costly and time-consuming

scanning electron microscope (SEM) with energy-dispersive X-ray spectroscopy (EDX) attachment. Since no correlation between the K-contents and luminescence properties could be found, we conclude that for single grain measurements in feldspars with heterogeneous K-contents the internal dose rate estimation should not be based on an average literature-based value. Further, we cannot recommend using SEM-EDX measurements to overcome the problem, since they are costly and time consuming. Therefore, the internal dose rate determination for single grain luminescence measurements remains a challenge.

When dealing with geochemically heterogeneous feldspars which give few suitable luminescence signals during single grain pIRIR measurements, we recommend using the rcsRxSGC method with a sR in the size of the expected D_e and rc consisting of a recuperation point, a recycling point with a size smaller than the expected D_e, and an additional dose point with a size of D_0 to $2D_0$ of the xSGC. Yet a feasible solution for single grain K-content measurements is still needed.

7. Glossary

dataset A	dataset build with five samples from the Atacama Desert (cf. Tab. 1)
dataset X	dataset build with five samples from outside the Atacama Desert (cf. Tab. 1)
D_i	regenerative dose
D_{r1}	regenerative dose from which the L_x/T_x value is used for fitting onto the SGC
L_{sR} and T_{sR}	synthetic L_{r1}/T_{r1} signal used for fitting onto the SGC
L_{r1} and T_{r1}	signal and test dose signal used for fitting onto the SGC
rc	reduced measurement cycles
rcsRxSGC	SGC build with dataset X and data from A with reduced cycles and synthetic regenerative dose used for fitting
r_s	Spearman rank correlation coefficient
SGC	standardised growth curve
sR	synthetic regenerative dose
xSGC	SGC build with dataset X

Declaration of competing interest

The authors declare that they have no known competing financial interests or personal relationships that could have appeared to influence the work reported in this paper.

Acknowledgements

This project is affiliated to the Collaborative Research Centre (CRC) 1211 "Earth – Evolution at the Dry Limit" (Grant-No.: 268236062) funded by the German Research Foundation (Deutsche Forschungsgemeinschaft, DFG), Germany. We would like to thank our colleagues who kindly supplied us with sample material. We thank Georgina E. King (Université de Lausanne) for MBT-I-2430, Benny Guralnik (Technical University of Denmark) for KTB-383-C, Dominik Brill (University of Cologne) for PAG-6-4b, PAG-6-6b and ISM-7, Simon M. May (University of Cologne) for CSA-1-2-2 and LAGU-1-1 and Aline Zinelabedin (University of Cologne) for ARO-18-08 LP. SR would like to thank Ulrike Hardenbicker for guidance in the field during which sample ABLR-1 was taken, and for hosting her at the University of Regina, Canada. We also thank Kathrin Jung (University of Cologne) for embedding our grains in resin and Hanna Cieszynski (University of Cologne) for the SEM-EDX measurements. SR acknowledges support by the European Union's Horizon Europe research and innovation programme (RECREATE, grant no. 101103587) during co-writing and editing the manuscript. The sampling campaign during which sample ABLR-1 was sampled was financially supported by a Female Research Grant from the Faculty of Mathematics and Natural Sciences, University of Cologne, awarded to SR.

References

Amundson, R., Richter, D.D., Humphreys, G.S., Jobbágy, E.G., Gaillardet, J., 2007. Coupling between Biota and Earth Materials in the Critical Zone. Elements 3, 327–332. https://doi.org/10.2113/gselements.3.5.327

Balian, H.G., Eddy, N.W., 1977. Figure-of-merit (FOM), an improved criterion over the normalized chi-squared test for assessing goodness-of-fit of gamma-ray spectral peaks. Nuclear Instruments and Methods 145, 389–395. https://doi.org/10.1016/0029-554X(77)90437-2

Bartz, M., Duval, M., Brill, D., Zander, A., King, G.E., Rhein, A., Walk, J., Stauch, G., Lehmkuhl, F., Brückner, H., 2020a. Testing the potential of K-feldspar pIR-IRSL and quartz ESR for dating coastal alluvial fan complexes in arid environments. Quaternary International, Electron spin resonance (ESR) dating in Quaternary studies: evolution, recent advances and applications 556, 124–143. https://doi.org/10.1016/j.quaint.2020.03.037

Bartz, M., Walk, J., Binnie, S.A., Brill, D., Stauch, G., Lehmkuhl, F., Hoffmeister, D., Brückner, H., 2020b. Late Pleistocene alluvial fan evolution along the coastal Atacama Desert (N Chile). Global and Planetary Change 190, 103091. https://doi.org/10.1016/j.gloplacha.2019.103091

Bonnet, S., Reimann, T., Wallinga, J., Lague, D., Davy, P., Lacoste, A., 2019. Landscape dynamics revealed by luminescence signals of feldspars from fluvial terraces. Sci Rep 9, 8569. https://doi.org/10.1038/s41598-019-44533-4

Brill, D., Reimann, T., Wallinga, J., May, S.M., Engel, M., Riedesel, S., Brückner, H., 2018. Testing the accuracy of feldspar single grains to date late Holocene cyclone and tsunami deposits. Quaternary Geochronology 48, 91–103. https://doi.org/10.1016/j.quageo.2018.09.001

Del Río, I., Sawakuchi, A.O., González, G., 2019. Luminescence dating of sediments from central Atacama Desert, northern Chile. Quaternary Geochronology 53, 101002. https://doi.org/10.1016/j.quageo.2019.05.001

Diederich, J.L., Wennrich, V., Bao, R., Büttner, C., Bolten, A., Brill, D., Buske, S., Campos, E., Fernández-Galego, E., Gödickmeier, P., Ninnemann, L., Reyers, M., Ritter, B., Ritterbach, L., Rolf, C., Scheidt, S., Dunai, T.J., Melles, M., 2020. A 68 ka precipitation record from the hyperarid core of the Atacama Desert in northern Chile. Global and Planetary Change 184, 103054. https://doi.org/10.1016/j.gloplacha.2019.103054

Dietrich, W.E., Perron, J.T., 2006. The search for a topographic signature of life. Nature 439, 411–418. https://doi.org/10.1038/nature04452

Finch, A.A., Klein, J., 1999. The causes and petrological significance of cathodoluminescence emissions from alkali feldspars. Contrib Mineral Petrol 135, 234–243. https://doi.org/10.1007/s004100050509

Fitzsimmons, K.E., Rhodes, E.J., Barrows, T.T., 2010. OSL dating of southeast Australian quartz: A preliminary assessment of luminescence characteristics and behaviour. Quaternary Geochronology, 12th International Conference on Luminescence and Electron Spin Resonance Dating (LED 2008) 5, 91–95. https://doi.org/10.1016/j.quageo.2009.02.009

Fuchs, M., Owen, L.A., 2008. Luminescence dating of glacial and associated sediments: review, recommendations and future directions. Boreas 37, 636–659. https://doi.org/10.1111/j.1502-3885.2008.00052.x

Garcia-Guinea, J., Townsend, P.D., Sanchez-Muñoz, L., Rojo, J.M., 1999. Ultraviolet-blue ionic luminescence of alkali feldspars from bulk and interfaces. Phys Chem Min 26, 658–667. https://doi.org/10.1007/s002690050231

Geake, J.E., Walker, G., Mills, A.A., Garlick, G.F.J., 1972. Luminescence of lunar material excited by electrons. Proceedings of the Lunar Science Conference 2971–2977.

Giardino, J.R., Houser, C., 2015. Principles and dynamics of the critical zone, Developments in earth surface processes. Elsevier, Amsterdam Boston.

Guralnik, B., Jain, M., Herman, F., Ankjærgaard, C., Murray, A.S., Valla, P.G., Preusser, F., King, G.E., Chen, R., Lowick, S.E., Kook, M., Rhodes, E.J., 2015. OSL-thermochronometry of feldspar from the KTB borehole, Germany. Earth and Planetary Science Letters 423, 232–243. https://doi.org/10.1016/j.epsl.2015.04.032

Huntley, D.J., Baril, M.R., 1997. The K content of the K-feldspars being measured in optical dating or in thermoluminescence dating. Ancient TL 15, 3.

Kars, R.H., Reimann, T., Wallinga, J., 2014. Are feldspar SAR protocols appropriate for post-IR IRSL dating? Quaternary Geochronology 22, 126–136. https://doi.org/10.1016/j.quageo.2014.04.001

Kook, M.H., Murray, A.S., Lapp, T., Denby, P.H., Ankjærgaard, C., Thomsen, K., Jain, M., Choi, J.H., Kim, G.H., 2011. A portable luminescence dating instrument. Nuclear Instruments and Methods in Physics Research Section B: Beam Interactions with Materials and Atoms 269, 1370–1378. https://doi.org/10.1016/j.nimb.2011.03.014

Lambert, R., 2018. Investigating thermal decay in K-feldspar for the application of IRSL thermochronometry on the Mont Blanc massif. University of Lausanne, Lausanne.

Lapp, T., Jain, M., Thomsen, K.J., Murray, A.S., Buylaert, J.-P., 2012. New luminescence measurement facilities in retrospective dosimetry. Radiation Measurements 47, 803–808. https://doi.org/10.1016/j.radmeas.2012.02.006

Li, B., Jacobs, Z., Roberts, R.G., 2016. Investigation of the applicability of standardised growth curves for OSL dating of quartz from Haua Fteah cave, Libya. Quaternary Geochronology 35, 1–15. https://doi.org/10.1016/j.quageo.2016.05.001

Li, B., Jacobs, Z., Roberts, R.G., Li, S.-H., 2018. Single-grain dating of potassium-rich feldspar grains: Towards a global standardised growth curve for the post-IR IRSL signal. Quaternary Geochronology 45, 23–36. https://doi.org/10.1016/j.quageo.2018.02.001

Li, B., Roberts, R.G., Jacobs, Z., Li, S.-H., 2015a. Potential of establishing a 'global standardised growth curve' (gSGC) for optical dating of quartz from sediments. Quaternary Geochronology 27, 94–104. https://doi.org/10.1016/j.quageo.2015.02.011

Li, B., Roberts, R.G., Jacobs, Z., Li, S.-H., Guo, Y.-J., 2015b. Construction of a 'global standardised growth curve' (gSGC) for infrared stimulated luminescence dating of K-feldspar. Quaternary Geochronology 27, 119–130. https://doi.org/10.1016/j.quageo.2015.02.010

Li, S.-H., Wintle, A.G., 1992. Luminescence sensitivity change due to bleaching of sediments. International Journal of Radiation Applications and Instrumentation. Part D. Nuclear Tracks and Radiation Measurements 20, 567–573. https://doi.org/10.1016/1359-0189(92)90006-H

Mahan, S.A., Rittenour, T.M., Nelson, M.S., Ataee, N., Brown, N., DeWitt, R., Durcan, J., Evans, M., Feathers, J., Frouin, M., Guérin, G., Heydari, M., Huot, S., Jain, M., Keen-Zebert, A., Li, B., López, G.I., Neudorf, C., Porat, N., Rodrigues, K., Sawakuchi, A.O., Spencer, J.Q.G., Thomsen, K., 2022. Guide for interpreting and reporting luminescence dating results. GSA Bulletin. https://doi.org/10.1130/B36404.1

May, S.M., Meine, L., Hoffmeister, D., Brill, D., Medialdea, A., Wennrich, V., Gröbner, M., Schulte, P., Steininger, F., Deprez, M., de Kock, T., Bubenzer, O., 2020. Origin and timing of past hillslope activity in the hyper-arid core of the Atacama Desert – The formation of fine sediment lobes along the Chuculay Fault System, Northern Chile. Global and Planetary Change 184, 103057. https://doi.org/10.1016/j.gloplacha.2019.103057

May, S.M., Zander, A., Francois, J.P., Kelletat, D., Pötsch, S., Rixhon, G., Brückner, H., 2015. Chronological and geoarchaeological investigations on an anthropogenic shell accumulation layer in the Longotoma dune field (Central Chile). Quaternary International 367, 32–41. https://doi.org/10.1016/j.quaint.2014.06.005

Mueller, D., Preusser, F., 2022. Investigating the applicability of a standardised growth curve approach on Middle Pleistocene sediments from northern Switzerland. Quaternary Geochronology 67, 101238. https://doi.org/10.1016/j.quageo.2021.101238

Murray, A.S., Wintle, A.G., Wallinga (INVITED), J., 2002. Dose Estimation Using Quartz OSL in the Non-linear Region of the Growth Curve. Radiation Protection Dosimetry 101, 371–374. https://doi.org/10.1093/oxfordjournals.rpd.a006004

Oeser, R.A., Stroncik, N., Moskwa, L.-M., Bernhard, N., Schaller, M., Canessa, R., van den Brink, L., Köster, M., Brucker, E., Stock, S., Fuentes, J.P., Godoy, R., Matus, F.J., Oses Pedraza, R., Osses McIntyre, P., Paulino, L., Seguel, O., Bader, M.Y., Boy, J., Dippold, M.A., Ehlers, T.A., Kühn, P., Kuzyakov, Y., Leinweber, P., Scholten, T., Spielvogel, S., Spohn, M., Übernickel, K., Tielbörger, K., Wagner, D., von Blanckenburg, F., 2018. Chemistry and microbiology of the Critical Zone along a steep climate and vegetation gradient in the Chilean Coastal Cordillera. CATENA 170, 183–203. https://doi.org/10.1016/j.catena.2018.06.002

O'Gorman, K., Tanner, D., Sontag-González, M., Li, B., Brink, F., Jones, B.G., Dosseto, A., Jatmiko, Roberts, R.G., Jacobs, Z., 2021. Composite grains from volcanic terranes: Internal dose rates of supposed 'potassium-rich' feldspar grains used for optical dating at Liang Bua, Indonesia. Quaternary Geochronology 64, 101182. https://doi.org/10.1016/j.quageo.2021.101182

Peng, J., Li, B., 2017. Single-aliquot Regenerative-Dose (SAR) and Standardised Growth Curve (SGC) Equivalent Dose Determination in a Batch Model Using the R Package 'numOSL' 35.

Peng, J., Li, B., More, J., Garbow, B., Hillstrom, K., Burkardt, J., Gilbert, P., Varadhan, R., 2018. numOSL: Numeric Routines for Optically Stimulated Luminescence Dating.

Prescott, J.R., Fox, P.J., 1993. Three-dimensional thermoluminescence spectra of feldspars. J. Phys. D: Appl. Phys. 26, 2245–2254. https://doi.org/10.1088/0022-3727/26/12/024

Reimann, T., Román-Sánchez, A., Vanwalleghem, T., Wallinga, J., 2017. Getting a grip on soil reworking – Single-grain feldspar luminescence as a novel tool to quantify soil reworking rates. Quaternary Geochronology 42, 1–14. https://doi.org/10.1016/j.quageo.2017.07.002

Riedesel, S., Bell, A.M.T., Duller, G.A.T., Finch, A.A., Jain, M., King, G.E., Pearce, N.J., Roberts, H.M., 2021. Exploring sources of variation in thermoluminescence emissions and anomalous

fading in alkali feldspars. Radiation Measurements 141, 106541. https://doi.org/10.1016/j.radmeas.2021.106541

Riedesel, S., King, G.E., Prasad, A.K., Kumar, R., Finch, A.A., Jain, M., 2019. Optical determination of the width of the band-tail states, and the excited and ground state energies of the principal dosimetric trap in feldspar. Radiation Measurements 125, 40–51. https://doi.org/10.1016/j.radmeas.2018.08.019

Ritter, B., Wennrich, V., Medialdea, A., Brill, D., King, G., Schneiderwind, S., Niemann, K., Fernández-Galego, E., Diederich, J., Rolf, C., Bao, R., Melles, M., Dunai, T.J., 2019. "Climatic fluctuations in the hyperarid core of the Atacama Desert during the past 215 ka." Sci Rep 9, 5270. https://doi.org/10.1038/s41598-019-41743-8

Román-Sánchez, A., Laguna, A., Reimann, T., Giráldez, J.V., Peña, A., Vanwalleghem, T., 2019a. Bioturbation and erosion rates along the soil-hillslope conveyor belt, part 2: Quantification using an analytical solution of the diffusion–advection equation. Earth Surface Processes and Landforms 44, 2066–2080. https://doi.org/10.1002/esp.4626

Román-Sánchez, A., Reimann, T., Wallinga, J., Vanwalleghem, T., 2019b. Bioturbation and erosion rates along the soil-hillslope conveyor belt, part 1: Insights from single-grain feldspar luminescence. Earth Surface Processes and Landforms 44, 2051–2065. https://doi.org/10.1002/esp.4628

Sawakuchi, A.O., Blair, M.W., DeWitt, R., Faleiros, F.M., Hyppolito, T., Guedes, C.C.F., 2011. Thermal history versus sedimentary history: OSL sensitivity of quartz grains extracted from rocks and sediments. Quaternary Geochronology 6, 261–272. https://doi.org/10.1016/j.quageo.2010.11.002

Smedley, R.K., Duller, G.A.T., Pearce, N.J.G., Roberts, H.M., 2012. Determining the K-content of single-grains of feldspar for luminescence dating. Radiation Measurements, Proceedings of the 13th International Conference on Luminescence and Electron Spin Resonance Dating, 10–14 July, 2011, Toruń, Poland 47, 790–796. https://doi.org/10.1016/j.radmeas.2012.01.014

Sontag-González, M., Li, B., O'Gorman, K., Sutikna, T., Jatmiko, Jacobs, Z., Roberts, R.G., 2021. Establishing a pIRIR procedure for De determination of composite mineral grains from volcanic terranes: A case study of sediments from Liang Bua, Indonesia. Quaternary Geochronology 65, 101181. https://doi.org/10.1016/j.quageo.2021.101181

Spearman, C., 1904. The proof and measurement of association between two things. The American Journal of Psychology 15, 72–101. https://doi.org/10.2307/1412159

Spooner, N.A., 1992. Optical dating: Preliminary results on the anomalous fading of luminescence from feldspars. Quaternary Science Reviews, Proceedings of the 6th International Specialist Seminar on Thermoluminescence and Electron Spin Resonance Dating 11, 139–145. https://doi.org/10.1016/0277-3791(92)90055-D

Starke, J., Ehlers, T.A., Schaller, M., 2020. Latitudinal effect of vegetation on erosion rates identified along western South America. Science 367, 1358–1361. https://doi.org/10.1126/science.aaz0840

Steffen, D., Preusser, F., Schlunegger, F., 2009. OSL quartz age underestimation due to unstable signal components. Quaternary Geochronology 4, 353–362. https://doi.org/10.1016/j.quageo.2009.05.015

Tchakerian, V., Pease, P., 2015. Chapter 14 - The Critical Zone in Desert Environments, in: Giardino, J.R., Houser, C. (Eds.), Developments in Earth Surface Processes. Elsevier, pp. 449–472. https://doi.org/10.1016/B978-0-444-63369-9.00014-8

Thomsen, K.J., Murray, A.S., Jain, M., Bøtter-Jensen, L., 2008. Laboratory fading rates of various luminescence signals from feldspar-rich sediment extracts. Radiation Measurements 43, 1474–1486. https://doi.org/10.1016/j.radmeas.2008.06.002

Tokuyasu, K., Tanaka, K., Tsukamoto, S., Murray, A., 2010. The Characteristics of OSL Signal from Quartz Grains Extracted from Modern Sediments in Japan.

Veit, H., Preusser, F., Trauerstein, M., 2015. The Southern Westerlies in Central Chile during the two last glacial cycles as documented by coastal aeolian sand deposits and intercalating palaeosols. CATENA 134, 30–40. https://doi.org/10.1016/j.catena.2014.11.002

Wei, T., Simko, V., 2023. R package "corrplot": Visualization of a Correlation Matrix. (Version 0.92),.

Zinelabedin, A., Riedesel, S., Reimann, T., Ritter, B., Dunai, T.J., 2022. Testing the potential of using coarse-grain feldspars for post-IR IRSL dating of calcium sulphate-wedge growth in the Atacama Desert. Quaternary Geochronology 101341. https://doi.org/10.1016/j.quageo.2022.101341

This paper is a **non-peer reviewed preprint** submitted to EarthArXiv and this paper is under revision at the Journal **Quaternary Geochronology**.

Supplementary Material

Testing the applicability of standardised growth curves (SGC) for chemically heterogeneous single-grain feldspars from the Atacama Desert, Chile

Linda A.E. Maßon[1*], Svenja Riedesel[1,2], Anja Zander[1], Mariana Sontag-González[3,4], Tony Reimann[1]

[1] Institute of Geography, University of Cologne, Germany
[2] Radiation Physics Division, Department of Physics, Technical University of Denmark, Denmark
[3] Institute of Geography, Justus-Liebig-University Gießen, Germany
[4] Department of Geosciences, Stony Brook University, NY 11794-2100, USA

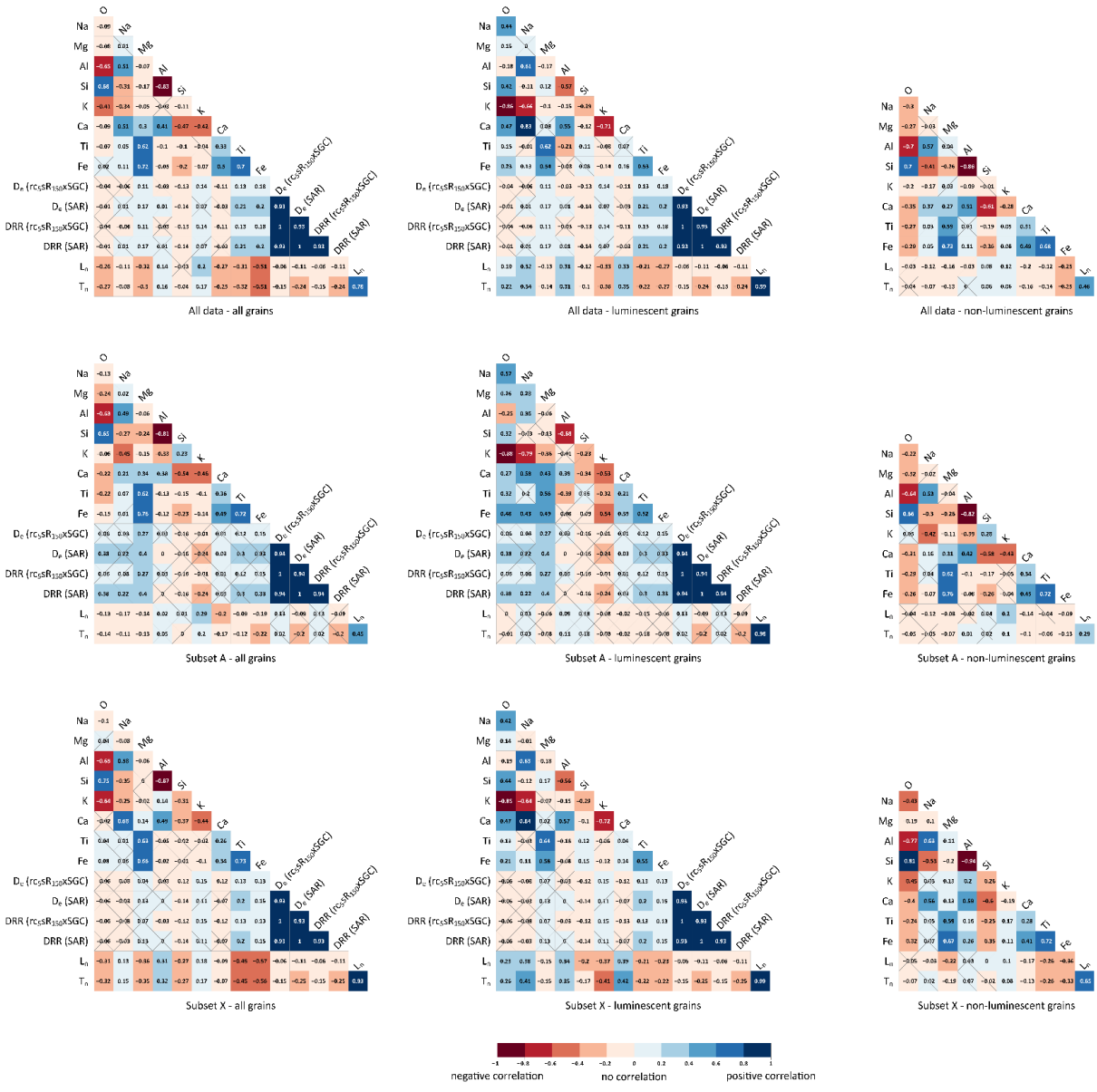

Fig. S1: correlation matrices of the complete dataset (subset A + X) in the first row, subset A in the second row and subset X in the third row, for all grains in the first column, luminescent grains in the second column and non-luminescent grains in the third column. Numbers in the squares represent Spearman's rank correlation coefficient values and their colour the strength of the correlation. For not significant correlations with a p-value above 0.05 % the squares are x-ed out.

775 *Table S1: summary of grain rejection for all ten samples for the SAR procedure, the SGC method (samples 1-5) and he xSGC method (samples 6-10) for the full data sets using all SAR cycles.*

776

Description	ARO-18-08-LP	CSA-1-2-2	LAGU-1-1	PAG-6-4b	PAG-6-6b	ABLR-1	HAM-5	ISM-7	KTB-383-C	MBT-I-2430
Total number of analysed grains	500	500	500	500	500	500	500	500	500	500
Rejection criterion: Tn below 3 σ BG	385	421	268	433	416	314	173	360	62	3
Rejection criterion: RSE of Tn exceeds 25 %	75	52	67	58	52	104	65	74	29	4
Rejection criterion: recycling ratio 1 outsides [0.9:1.1]	3	1	9	1	2	8	13	2	43	52
Rejection criterion: recycling ratio 2 outsides [0.9:1.1]	0	0	0	0	0	0	0	0	0	0
Rejection criterion: recycling ratio 3 outsides [0.9:1.1]	0	0	0	0	0	0	0	0	0	0
Rejection criterion: recuperation 1 exceeds 10 %	0	0	0	0	1	1	1	0	6	0
Rejection criterion: recuperation 2 exceeds 10 %	0	0	0	0	0	0	0	0	0	0
Function fitGrowth(): improper input argument	0	0	0	0	0	0	0	0	0	0
Function fitGrowth(): failed in growth curve fitting	0	0	0	1	0	3	0	0	1	0
Rejection criterion: FOM of growth curve exceeds 10%	23	22	90	6	11	41	65	31	62	74
Rejection criterion: RCS of growth curve exceeds 10	1	0	4	0	10	5	75	1	201	58
Total number of rejected grains	487	496	438	499	492	476	392	468	404	191
Total number of accepted grains	13	4	62	1	8	24	108	32	96	309

777 *Table S2: summary of the results for dataset A using the sRxSGC approach, in relation to the De calculated with the SAR approach and to a dose recovery ratio (DRR) of 1.*

synthetic regenerative dose (sR) size used in the sRxSGC approach	50	100	125	150	175	200	300	800
n D_e	88	88	88	88	88	88	88	88
n D_e common grains sRxSGC & SAR	86	86	86	86	86	86	86	87
In unity within 10 %	69	83	86	85	76	69	36	11
In unity within 1 σ	16	3	0	1	10	16	36	24
In unity within 2 σ	1	0	0	0	0	1	12	28
Not in unity	0	0	0	0	0	0	2	24
NA in either sRxSGC or SAR	2	2	2	2	2	2	2	1
Differences in D_e								
Min	0.37	0.00	0.00	0.03	0.01	0.02	0.07	1.58
Max	46.63	25.10	19.31	16.53	25.31	34.31	87.21	282.54
Mean	9.36	3.86	2.42	2.65	4.81	7.48	19.61	59.99
sd	9.84	4.96	3.16	3.10	4.74	7.00	16.42	50.05
CV	1.05	1.29	1.31	1.17	0.99	0.94	0.84	0.83
DRR (all grains)								
DRR between 0.9-1.1	25	20	26	30	30	33	29	15
DRR with 1 σ error between 0.9-1.1	28	35	31	26	30	28	34	20
DRR with 1 σ error not between 0.9-1.1	33	31	29	30	26	25	23	52
NA in either	2	2	2	2	2	2	2	1
Mean DRR	0.87	0.86	0.87	0.89	0.9	0.91	0.98	1.19
DRR (common grains)								
DRR between 0.9-1.1	25	20	26	30	30	33	29	15
DRR with 1 σ error between 0.9-1.1	28	35	31	26	30	28	34	20
DRR with 1 σ error not between 0.9-1.1	33	31	29	30	26	25	23	52
NA in either	2	2	2	2	2	2	2	1
Mean DRR	0.87	0.86	0.87	0.89	0.9	0.91	0.98	1.19
Correlation with SAR (r_s values)	0.9	0.99	0.99	0.99	0.97	0.94	0.76	0.21

778 *Table S3: summary of grain rejection for all ten samples for the SAR procedure, the SGC method (samples 1-5) and he xSGC method (samples 6-10) for reduced dataset using the cycles of rc5.*

Description	ARO-18-08-LP	CSA-1-2-2	LAGU-1-1	PAG-6-4b	PAG-6-6b	ABLR-1	HAM-5	ISM-7	KTB-383-C	MBT-I-2430
Total number of analysed aliquots (grains)	500	500	500	500	500	500	500	500	500	500
Rejection criterion: Tn below 3 sigma BG	385	421	268	433	416	314	173	360	62	3
Rejection criterion: RSE of Tn exceeds 25%	75	52	67	58	52	104	65	74	29	4
Rejection criterion: recycling ratio 1 outsides [0.9:1.1]	3	1	9	1	2	8	13	2	43	52
Rejection criterion: recycling ratio 2 outsides [0.9:1.1]	0	0	0	0	0	0	0	0	0	0
Rejection criterion: recycling ratio 3 outsides [0.9:1.1]	0	0	0	0	0	0	0	0	0	0
Rejection criterion: recuperation 1 exceeds 10%	0	0	0	0	1	1	1	0	6	0
Rejection criterion: recuperation 2 exceeds 10%	0	0	0	0	1	0	0	0	0	0
Function fitGrowth(): improper input argument	0	0	0	0	0	0	0	0	0	0
Function fitGrowth(): failed in growth curve fitting	0	0	0	1	0	2	0	0	0	0
Rejection criterion: FOM of growth curve exceeds 10%	7	9	12	1	2	11	9	5	3	4
Rejection criterion: RCS of growth curve exceeds 10	0	0	0	0	1	0	7	1	27	7
Total number of rejected aliquots (grains)	470	483	356	494	475	440	268	442	170	70
Total number of accepted aliquots (grains)	30	17	144	6	25	60	232	58	330	430

779

Table S4: summary of the results for dataset A using the rcsR150xSGC approach, in relation to the De calculated with the SAR approach and to a dose recovery ratio (DRR) of 1. Headers indicating the size of the dose (Di) of the used cycles, with the first 150 being the "natural" cycle. The abbreviations refer to Table 3.

Reduced cycles used (sR = 150 Gy)	150-0-50-300	150-0-50-500	150-0-50-800	150-0-50-150-50	150-0-50-300-50	150-0-50-500-50	150-0-50-800-50	150-0-150-300-150	150-0-150-500-150	150-0-150-800-150
Abbreviation	**rc_1**	**rc_2**	**rc_3**	**rc_4**	**rc_5**	**rc_6**	**rc_7**	**rc_8**	**rc_9**	**rc_{10}**
n D_e	219	226	229	142	198	206	212	186	200	208
n D_e common grains $rcsR_{150}$xSGC & SAR	86	86	87	59	86	86	87	85	86	86
In unity within 10 %	68	53	48	41	72	69	64	62	63	63
In unity within 1 σ	18	33	38	18	14	17	22	22	22	22
In unity within 2 σ	0	0	1	0	0	0	1	1	1	1
Not in unity	0	0	0	0	0	0	0	0	0	0
NA in either $rcsR_{150}$xSGC or SAR	158	159	155	125	130	132	134	120	129	133
Differences in D_e										
Min	0.11	0.10	0.48	0.15	0.03	0.17	0.43	0.22	0.21	0.21
Max	45.08	92.96	163.44	38.78	29.37	66.85	72.05	33.63	33.63	33.63
Mean	9.00	12.21	15.33	8.70	7.40	8.74	11.43	9.98	9.85	9.85
sd	8.25	12.93	19.67	8.02	6.51	9.45	10.45	7.57	7.61	7.61
CV	0.92	1.06	1.28	0.92	0.88	1.08	0.91	0.76	0.77	0.77
DRR (all grains)										
DRR between 0.9-1.1	58	50	46	25	54	57	47	59	65	66
DRR with 1 σ error between 0.9-1.1	85	82	73	36	80	66	66	63	68	71
DRR with 1 σ error not between 0.9-1.1	75	93	110	53	63	82	99	62	66	67
NA in either	26	20	13	70	19	13	9	21	16	12
Mean DRR	0.91	0.88	0.88	0.78	0.9	0.89	0.87	0.95	0.98	0.99
DRR (common grains)										
DRR between 0.9-1.1	21	18	17	13	23	24	21	32	32	32
DRR with 1 σ error between 0.9-1.1	34	28	25	17	33	22	18	26	26	26
DRR with 1 σ error not between 0.9-1.1	31	40	45	29	30	40	48	27	28	28
NA in either	26	20	13	70	19	13	9	21	16	12
Mean DRR	0.88	0.87	0.86	0.79	0.87	0.85	0.84	0.91	0.9	0.9
Correlation with SAR (r_s values)	0.92	0.9	0.9	0.84	0.94	0.94	0.95	0.89	0.89	0.89

Table S5: summary of the SEM-EDX measurement results for the nine elements measured. For each element the results are given for subset A, subset X and the complete dataset. The table is further divided in all grains (upper third), luminescent grains (middle third) and the non-luminescent grains (bottom third).

All	O			Na			Mg			Al			Si			K			Ca			Ti			Fe		
Element	subset A	subset X	total	subset A	subset X	total	subset A	subset X	total	subset A	subset X	total	subset A	subset X	total	subset A	subset X	total	subset A	subset X	total	subset A	subset X	total	subset A	subset X	total
n measurements	1193	1135	2328	1193	1135	2328	1193	1135	2328	1193	1135	2328	1193	1135	2328	1193	1135	2328	1193	1135	2328	1193	1135	2328	1193	1135	2328
n (without 0)	1193	1135	2328	1158	978	2136	531	258	789	1185	1067	2252	1193	1135	2328	1152	1002	2154	1046	658	1704	519	325	844	1071	562	1633
Min	44.04	42.55	42.55	0	0	0	0	0	0	0	0	0	12.22	18.63	12.22	0	0	0	0	0	0	0	0	0	0	0	0
Min (without 0)	44.04	42.55	42.55	0.32	0.13	0.13	0.07	0.08	0.07	0.34	0.25	0.25	12.22	18.63	12.22	0.06	0.06	0.06	0.07	0.03	0.03	0.04	0.04	0.04	0.08	0.07	0.07
Max	55.37	56.25	56.25	8.51	9.02	9.02	15.00	6.68	15.00	30.93	23.84	30.93	48.19	49.02	49.02	13.98	14.68	14.68	11.97	13.27	13.27	3.22	4.71	4.71	8.57	17.69	17.69
Mean	48.02	47.70	47.87	3.33	2.65	3.00	0.39	0.14	0.26	9.33	8.54	8.94	32.29	34.94	33.58	3.40	4.21	3.80	1.80	1.09	1.45	0.16	0.13	0.15	1.28	0.60	0.95
sd	1.74	2.25	2.01	1.84	2.35	2.13	0.78	0.39	0.63	2.73	3.95	3.40	3.72	5.99	5.13	3.01	4.88	4.05	2.18	1.83	2.05	0.26	0.32	0.29	1.39	1.44	1.46
Coefficient of variation	0.04	0.05	0.04	0.55	0.89	0.71	2.01	2.90	2.40	0.29	0.46	0.38	0.12	0.17	0.15	0.89	1.16	1.07	1.21	1.68	1.41	1.61	2.42	1.97	1.08	2.42	1.53

luminescent	O			Na			Mg			Al			Si			K			Ca			Ti			Fe		
Element	subset A	subset X	total	subset A	subset X	total	subset A	subset X	total	subset A	subset X	total	subset A	subset X	total	subset A	subset X	total	subset A	subset X	total	subset A	subset X	total	subset A	subset X	total
n measurements	65	434	499	65	434	499	65	434	499	65	434	499	65	434	499	65	434	499	65	434	499	65	434	499	65	434	499
n (without 0)	65	434	499	65	402	467	6	29	35	65	420	485	65	434	499	65	410	475	36	209	245	6	28	34	37	88	125
Min	44.88	43.86	43.86	0.42	0	0	0	0	0	1.65	0	0.00	27.66	28.02	27.66	0.24	0	0	0	0	0	0	0	0	0	0	0
Min (without 0)	44.88	43.86	43.86	0.42	0.13	0.13	0.22	0.12	0.12	1.65	0.59	0.59	27.66	28.02	27.66	0.24	0.06	0.06	0.10	0.06	0.06	0.27	0.07	0.07	0.09	0.08	0.08
Max	52.53	54.42	54.42	7.7	9.015	9.015	1.67	2.31	2.31	17.05	14.44	17.05	44.23	48.72	48.72	13.33	14.63	14.63	4.42	5.46	5.46	1.13	1.34	1.34	2.45	8.81	8.81
Mean	46.5	46.63	46.62	2.44	2.87	2.82	0.06	0.03	0.03	9.91	9.74	9.76	31.86	33.03	32.88	8.38	6.84	7.04	0.48	0.73	0.69	0.04	0.02	0.02	0.28	0.11	0.13
sd	1.48	1.95	1.89	1.64	2.66	2.55	0.26	0.15	0.17	1.95	2.99	2.87	2.58	4.48	4.30	3.97	5.81	5.62	0.79	1.06	1.03	0.16	0.12	0.13	0.51	0.51	0.51
Coefficient of variation	0.03	0.04	0.04	0.67	0.93	0.91	3.94	5.66	5.32	0.20	0.31	0.29	0.08	0.14	0.13	0.47	0.85	0.80	1.63	1.47	1.49	3.84	5.46	5.13	1.82	4.72	3.93

non-luminescent	O			Na			Mg			Al			Si			K			Ca			Ti			Fe		
Element	subset A	subset X	total	subset A	subset X	total	subset A	subset X	total	subset A	subset X	total	subset A	subset X	total	subset A	subset X	total	subset A	subset X	total	subset A	subset X	total	subset A	subset X	total
n measurements	1128	701	1829	1128	701	1829	1128	701	1829	1128	701	1829	1128	701	1829	1128	701	1829	1128	701	1829	1128	701	1829	1128	701	1829
n (without 0)	1128	701	1829	1093	576	1669	525	229	754	1120	647	1767	1128	701	1829	1087	592	1679	1010	449	1459	513	297	810	1034	474	1508
Min	44.04	42.55	42.55	0	0	0	0	0	0	0	0	0	12.22	18.63	12.22	0	0	0	0	0	0	0	0	0	0	0	0
Min (without 0)	44.04	42.55	42.55	0.32	0.15	0.15	0.07	0.08	0.07	0.34	0.25	0.25	12.22	18.63	12.22	0.06	0.10	0.06	0.07	0.03	0.03	0.04	0.04	0.04	0.08	0.07	0.07
Max	55.37	56.25	56.25	8.51	8.46	8.51	15	6.68	15	30.925	23.84	30.925	48.19	49.02	49.02	13.975	14.68	14.68	11.97	13.27	13.27	3.22	4.71	4.71	8.57	17.69	17.69
Mean	48.1	48.37	48.21	3.39	2.51	3.05	0.40	0.20	0.33	9.29	7.79	8.72	32.31	36.12	33.77	3.11	2.59	2.91	1.87	1.32	1.66	0.17	0.20	0.18	1.34	0.90	1.17
sd	1.71	2.17	1.91	1.84	2.12	2.00	0.79	0.47	0.69	2.76	4.27	3.50	3.78	6.48	5.32	2.68	3.27	2.93	2.21	2.15	2.20	0.26	0.38	0.31	1.40	1.73	1.55
Coefficient of variation	0.04	0.04	0.04	0.54	0.85	0.66	1.96	2.33	2.12	0.30	0.55	0.40	0.12	0.18	0.16	0.86	1.26	1.01	1.18	1.63	1.33	1.56	1.89	1.73	1.04	1.92	1.32